FishTaxa - Journal of Fish Taxonomy
Vol 37, ISSN: 2458-942X

Synthesis and Antimicrobial Activity of Transition Metal Trimesate Complexes with Hydrazine

Reenu[1], Dr. Shilpi Shrivastava[2]
[1]Scholar, [2]Supervisor
Department Of Chemistry, Kalinga University
Naya Raipur, (India)
1 kundureenu60@gmail.com [2] dr.shilpi.shrivastava@kalingauniversity.ac.in

Abstract
Novel complexes of Mn(II), Co(II), Ni(II), Cu(II), and Zn(II) with trimesic acid (benzene-1,3,5-tricarboxylic acid) and hydrazine were synthesized and characterized. The complexes exhibited octahedral geometry, confirmed through electronic, FTIR, Raman, and EPR spectroscopic analyses. Thermal studies showed stepwise decomposition to form stable metal oxides, highlighting their potential as precursors for nanoparticle synthesis. Antibacterial and antifungal activity evaluations revealed that Zn(II) and Cu(II) complexes exhibited significant bioactivity against tested microbes, surpassing the free ligand. The study demonstrates the potential of these metal complexes for pharmaceutical and nanomaterial applications.

Keywords: Trimesic acid, hydrazine, transition metals, antimicrobial activity, thermal decomposition, nanoparticle precursors, EPR spectra.

Citation: Reenu, Dr. Shilpi Shrivastava. 2025. Synthesis and Antimicrobial Activity of Transition Metal Trimesate Complexes with Hydrazine. FishTaxa 37: 255-269

Introduction
The investigation of coordination complexes has captivated the attention of many researchers worldwide, owing to their intriguing molecular structures formed through interactions like metal-ligand coordination, stacking interactions, and hydrogen bonding [1-2]. These coordination compounds are expected to unveil applications as innovative materials featuring intriguing photophysical, photochemical, catalytic, sensing, magnetic, and electronic properties [3-4]. Hydrazine, the simplest diamine, even when protonated to form N2H5+, showcases its ability to bond with a wide range of metal ions, resulting in the formation of diverse salts with both mineral and carboxylic acids [5-8]. The chemistry surrounding hydrazine is remarkable due to its ability to form a variety of mixed-ligand complexes with transition metals. The stability and various properties of these complexes change considerably depending on the specific cations and anions involved [9-12]. Research into the thermal breakdown of metal carboxylates, utilising hydrazine as a co-ligand, is garnering significant attention from scientists [13-15]. These compounds serve as precursors for the synthesis of nanoparticle oxide materials and metal carbonates via straightforward pyrolysis reactions [16-17]. Neutral hydrazine interacts with metal ions predominantly through two unique mechanisms, specifically as either a monodentate or a bidentate bridging ligand (not solely bidentate to a single metal ion) [18-29]. In the presence of carboxylic acids, hydrazine can associate with metal ions in the form of the hydrazinium cation, as hydrazine exists as the hydrazinium cation under acidic conditions [20]. The core of the complex structure (neutral hydrazine or hydrazinium ion) depends on the plentiful presence of hydrazine, the acidity of the reaction environment, and the properties of the metallic ion involved [21]. Hydrazinium (mono-acidic hydrazine) complexes exhibit lower thermal stability compared to their neutral hydrazine counterparts; however, they present a fascinating structural complexity [23-25]. Trimesic acid, referred to as benzene-1,3,5-tricarboxylic acid, is a substance obtained from benzene featuring three carboxylic acid functional groups. Yttrium (III) tricarboxylates and those of rare earth elements (III) were successfully synthesised and characterized [26]. Recently developed transition metal–organic frameworks, one incorporating zinc (Zn) and the other featuring cadmium (Cd), were created and examined. The structures were developed utilising benzene-1,3,5-tricarboxylic acid alongside a luminous complex comprising terbium (Tb) and trimesic acid (TMA) [27]. The figures are eleven and twelve. The three recently created metal-trimesate compounds are referred to as [Cd3(TMA)2(H-PRZ)(H2O)3(OH)].The substances referenced include H2O (1), Cd2Na2(TMA)2(H2O)4 (2), and [Cd2Co(TMA)2(H2O)4] [28]. The fluorescence emissions in the solid state of ·2H2O (3) at room temperature were detected, attributed to its varied coordination structures. The information provided earlier inspired us to create novel compounds through the amalgamation of specific divalent transition metals (Cobalt, Nickel, Copper, Manganese, and Zinc) with 1,3,5-benzenetricarboxylic acid (Trimesic acid, H3tma) and hydrazine. Illustration 3.1 showcases the various potential synchronisation methods involving benzene tricarboxylic acid and metallic ions [29-30].

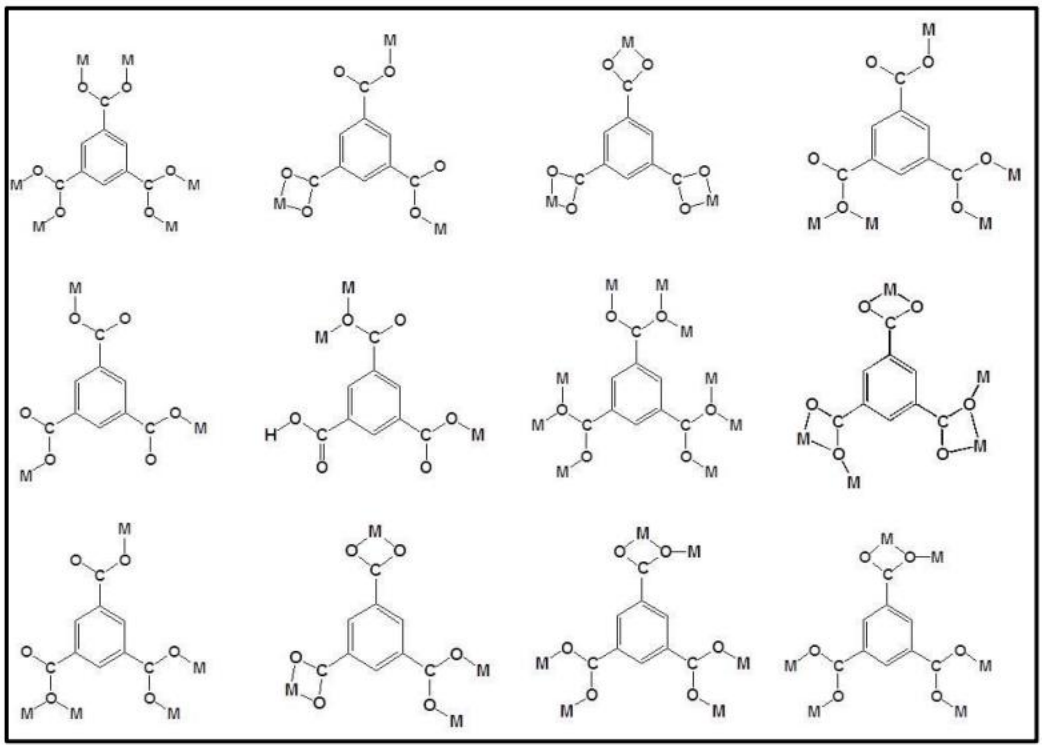

Source http://dx.doi.org/10.1016/j.jscs.2017.05.012

Fig. 1. Coordination fashions of trimesic acid (TMA).

Experimental section

2.1 Materials and methods

The substances utilised for the amalgamation and diverse physico-chemical methodologies employed in this study (Analytical, ESI-mass, electronic, FT-IR, Raman, EPR and EDX spectral, powder X-ray diffraction, TG–DTA, SEM and antimicrobial activities) are deliberated in Chapter II.

2.2 Synthesis of M(Htma)(N2H4)2, where M = Mn, Co, Ni, Cu and Zn

A total of 0.735 g (0.0035 mol) of Benzene-1,3,5-tricarboxylic acid was introduced into a 50 mL aqueous solution of hydrazine, which comprised 0.171 mL (0.0035 mol) of pure (99.5%) hydrazine hydrate. The blend was warmed in a water bath at 90 °C while being stirred until a clear, translucent solution was achieved. The corresponding metal nitrate (0.0035 mol, pH 5) was gradually introduced into an aqueous solution while being stirred consistently. The blend was subsequently subjected to reflux at a temperature of 80 °C for a duration of 12 hours. Manganic acetate tetrahydrate was utilised in the instance of Mn. The mixture's volume was diminished to approximately 20 mL by evaporating it over a water bath maintained at a temperature range of 80–90 °C. Following that, it was permitted to cool for a duration of 6 hours, during which the entire synthesis that was produced precipitated completely. The intricate chemical compound underwent a separation process through filtration, followed by a thorough washing with distilled water, ethanol, and hydrocarbon, and subsequently permitted to dry in the air .

Results and discussion

The synthesis of manganese, cobalt, nickel, copper, and zinc compounds was achieved by combining aqueous solutions of the respective metal nitrate hydrate, benzene-1,3,5-tricarboxylic acid, and hydrazine hydrate.

$$M(NO_3)_2.6H_2O + C_6H_3(COOH)_3 + 2N_2H_4.H_2O \rightarrow$$

$$[M(C_6H_3(COO)_2COOH)(N_2H_4)_2] + 2HNO_3 + 8H_2O \rightarrow \textbf{(1)}$$

where M = Co, Ni, and Zn.

$$Cu(NO_3)_2.3H_2O + C_6H_3(COOH)_3 + 2N_2H_4.H_2O \rightarrow$$

$$[Cu(C_6H_3(COO)_2COOH)(N_2H_4)_2] + 2HNO_3 + 5H_2O \rightarrow \textbf{(2)}$$

$$Mn(CH_3COO)_2.4H_2O + C_6H_3(COOH)_3 + 2N_2H_4.H_2O \rightarrow$$

The analytical information regarding the synthesised compounds can be located in Table 1. The recently synthesised metal hydrazine carboxylates exhibit limited solubility in water, alcohol, and various organic solvents; however, they demonstrate solubility in a mixed solvent comprising methanol and acetylacetone. The compositions of these complexes were established by analysing the elemental makeup (CHN), along with the detection of hydrazine and metallic components. Kindly consult Table 1 for additional information. To enhance the validation of the suggested chemical formula for the complexes, mass spectrometry analyses were conducted. Illustrated in Figure 3 are the mass spectra corresponding to the complexes of Cobalt(II), Nickel(II), Copper(II), Manganese(II), and Zinc(II).Please consider rewording your message or offering additional details to help me better understand your request. The mass spectra for the complexes of Cobalt(II), Nickel(II), Copper(II), Manganese(II), and Zinc(II) reveal molecular ion peaks at m/z 331.95 (m+H)+, 348.92 (m+NH4)+, 353.91 (m+NH4)+, 328.92 (m+H)+, and 336.76 (m–H)+, respectively. These peaks align with the anticipated formula weights of the respective Cobalt, Nickel, Copper, Manganese, and Zinc complexes. The prominent peak observed at 300.03 m/z in the mass spectrum of the Co(II) compound is attributed to the metal trimesate, following the elimination of the hydrazine fragment from the complex. The maximum observed at 317.84 m/z is linked to the fragment of cobalt ammonium trimesate. The prominent peak observed at 630.58 m/z in the mass spectrum of this complex is indicative of the dimeric form of the compound [Co(Htma)(N2H4)3Co(Htma)], which features a hydrazine bridge. Consequently, the mass spectroscopic findings enhance the analytical outcomes of the elemental (CHN), hydrazine, and metal compositions, validating the suggested molecular formula [M(Htma)(N2H4)2] for the compounds.

Table 1 Analytical data of ligand and complexes

Compound	Molecular weight	Color	Found (calculated)%				
			Carbon (CHN)	Hydrogen (CHN)	Nitrogen (CHN)	Metal (ICP-OES)	Hydrazine
Co(Htma)(N2H4)2	331.15	Light red	32.4(32.6)	3.8(3.6)	16.4(16.9)	17.2(17.7)	18.1(19.3)
Cu(Htma)(N2H4)2	335.77	Pale blue	30.1(30.4)	4.3(4.5)	15.5(15.7)	17.5(18.9)	18.4(19.0)
Ni(Htma)(N2H4)2	330.91	Green	30.7(30.9)	4.9(4.5)	16.2(16.0)	16.6(17.7)	18.5(19.3)
Mn(Htma)(N2H4)2	327.16	Dirty white	32.7(33.01)	3.1(3.6)	17.8(17.1)	15.5(16.7)	19.1(19.5)
Zn(Htma)(N2H4)2	337.63	Colorless	31.4(31.9)	3.5(3.6)	17.2(16.5)	18.2(19.3)	17.9(18.9)

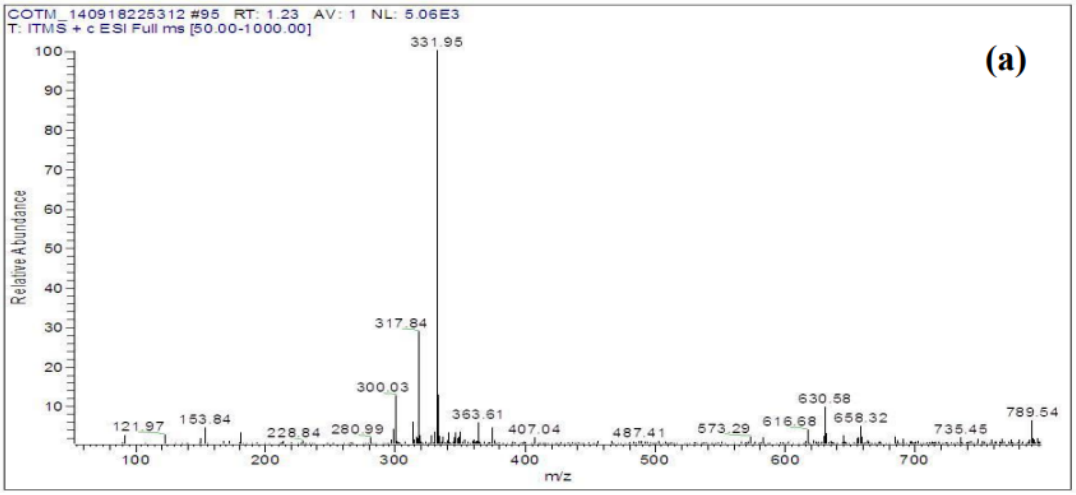

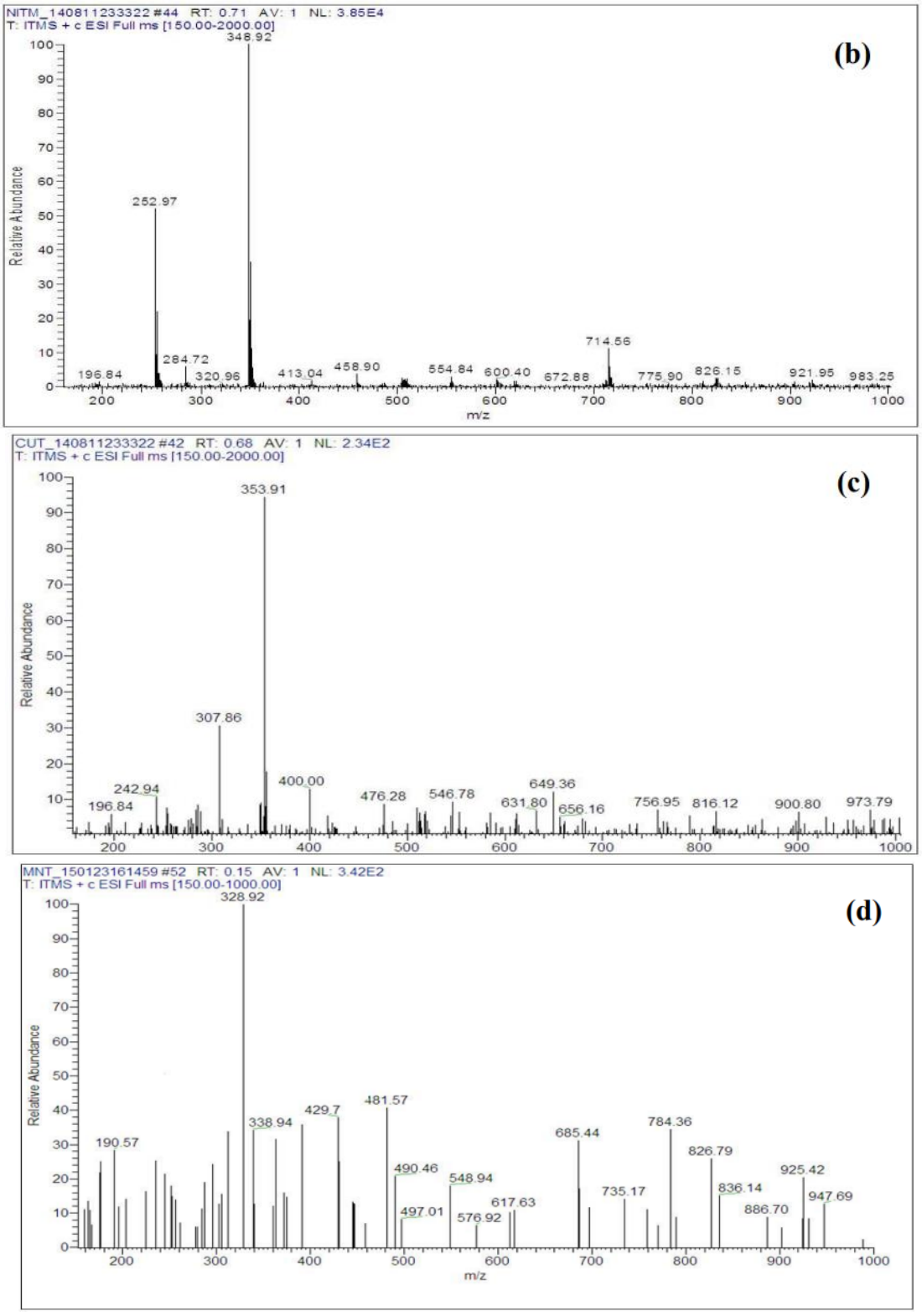

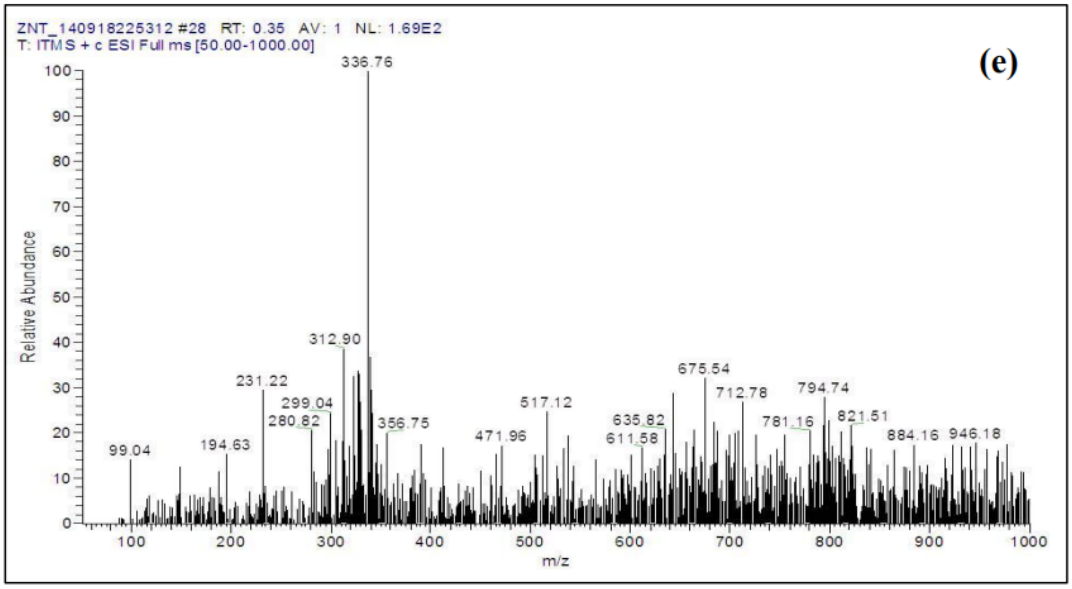

Fig. 2. Mass spectra of (a) Co(Htma)(N2H4)2, (b) Ni(Htma)(N2H4)2, (c) Cu(Htma)(N2H4)2, (d) Mn(Htma)(N2H4)2 and (e) Zn(Htma)(N2H4)2.

3.1 Electronic spectra

The nature of the ligand field encircling the metal ion and the configuration of the complexes were inferred from the positions and number of d–d bands observed in the electronic absorption spectral analyses. The electromagnetic spectra of the newly synthesised cobalt, nickel, and copper compounds, namely Co(Htma)(N2H4)2, Ni(Htma)(N2H4)2, and Cu(Htma)(N2H4)2, are illustrated in Fig. 3, highlighting shifts that suggest an octahedral environment enveloping these metal cations.

For example, the cobalt compound displays an extensive range between 17,500 and 24,000 cm–1 (λ maximum = 510 nm), which is ascribed to the transition from 4T1g (F) to 4T1g (P). The shoulder present in this outfit (around 480 nm) could have arisen from the splitting of the triply degenerate fundamental state (4T1g (F)) due to spin–orbit coupling. The transition from 4T1g (F) to 4A2g is hidden within the charge-transfer bands found in the ultraviolet spectrum, while the shift from 4T1g (F) to 4T2g is expected to appear in the near-infrared range.

The nickel compound exhibits two distinct spectra: one situated roughly within the range of 23,000–30,000 cm–1 (λ max = 400 nm) and the other falling between approximately 13,000–14,800 cm–1 (λ max = 722 nm). These are attributed to the transitions 3A2g → 3T1g (P) (3) and 3A2g → 3T1g (F) (2), respectively. In general, octahedral Ni(II) complexes display the transition from 3A2g to 3T2g within the near-infrared (NIR) region. The absorption band around ~655 nm arises from the spin-forbidden transition of 3A2g to 1Eg, which has increased in intensity due to the nearby spin-allowed transition. Utilising the specified transition frequencies, the Racah inter-electronic repulsion parameter, B', was calculated and found to be 929 cm–1. The reduced B' value for the compound, when contrasted with the independent ion B value (1080 for Ni2+), suggests a covalency factor 'α' (where α = B'/B) for the Ni(II) compound. This indicates that the interactions between the metal and ligand exhibit a significant degree of covalent character. By employing the B' value, the energy associated with ligand field partitioning, denoted as 10Dq, was calculated and found to be 8,305 cm–1.

The copper compound exhibits a spectrum around 12,500–20,408 cm–1, which arises from the 2Eg → 2T2g shift. In a hexacoordinate Cu(II) compound, the eg level of the 2D independent particle basic state will divide into B1g and A1g levels, while the t2g level divides into B2g and Eg levels. Hence, three rotate-permitted changes are anticipated in the observable and nearby-infrared area, but they are exceedingly proximate in energy and frequently manifest in the shape of one extensive band casing.

The Mn(II) and Zn(II) compounds do not exhibit any d-d bands in the visible area, as anticipated for semi- and completely-filled electronic setups of the metallic compounds.

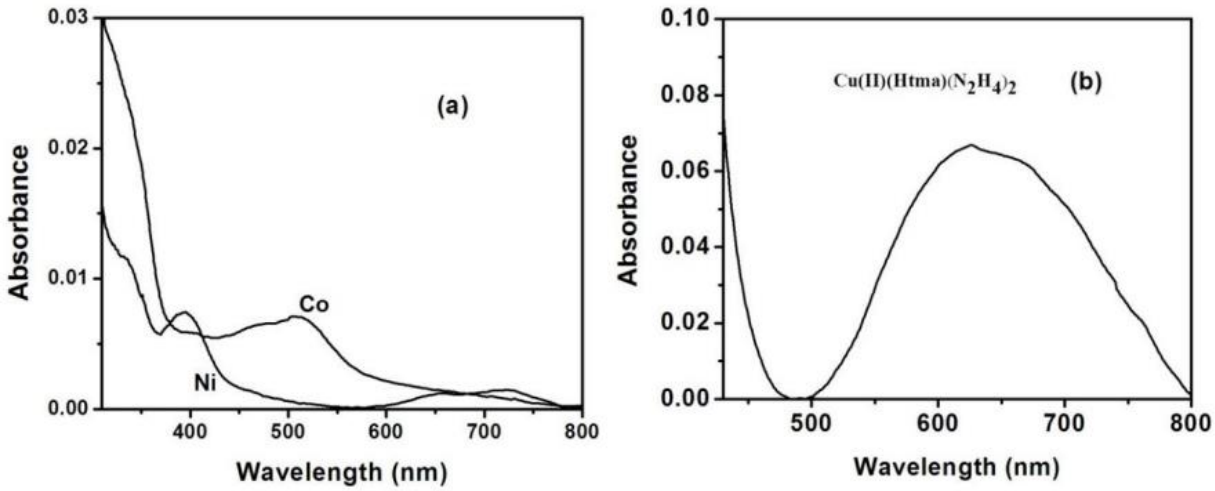

Fig. 3. Electronic Spectra of (a) Co(II)(Htma)(N2H4)2 and Ni(II)(Htma)(N2H4)2, and (b) Cu(II)(Htma)(N2H4)2.

3.2 Infrared spectra

Standard FTIR spectra observed for the compounds Co(Htma)(N2H4)2, Ni(Htma)(N2H4)2, Cu(Htma)(N2H4)2, Mn(Htma)(N2H4)2, and Zn(Htma)(N2H4)2 are exhibited in Fig. 4, and the significant IR absorption wavelengths of the synthesised compounds are enumerated in Table 2. All the arranged complexes exhibit IR bands in the area 3273–3296 cm–1, which are ascribed to N–H stretching frequencies of the hydrazine components. The disproportionate and balanced carboxylate vibrations of all the complexes are observed in the range 1612–1640 and 1363–1372 cm–1, correspondingly, with a Δ between them of 241–277 cm–1, indicating the monodentate coordination of each carboxylate group in the trimesic acid. The N–N oscillation frequency of hydrazine groups detected at 950–985 cm–1 suggests that the hydrazine groups are present as connecting dual-toothed ligands.

Table 2 Infrared spectral data (cm–1)

Compound	$\nu_{(N-H)}$	$\nu_{asym(COO^-)}$	$\nu_{sym(COO^-)}$	$\Delta\nu = (\nu_{asym(COO^-)} - \nu_{sym(COO^-)})$	$\nu_{(N-N)}$	$\nu_{(M-O)}$
$Co(Htma)(N_2H_4)_2$	3289	1612	1371	241	983	516
$Ni(Htma)(N_2H_4)_2$	3296	1640	1363	277	979	550
$Cu(Htma)(N_2H_4)_2$	3273	1626	1372	254	985	558
$Mn(Htma)(N_2H_4)_2$	-	1630	1372	258	950	533
$Zn(Htma)(N_2H_4)_2$	3280	1616	1367	249	970	563

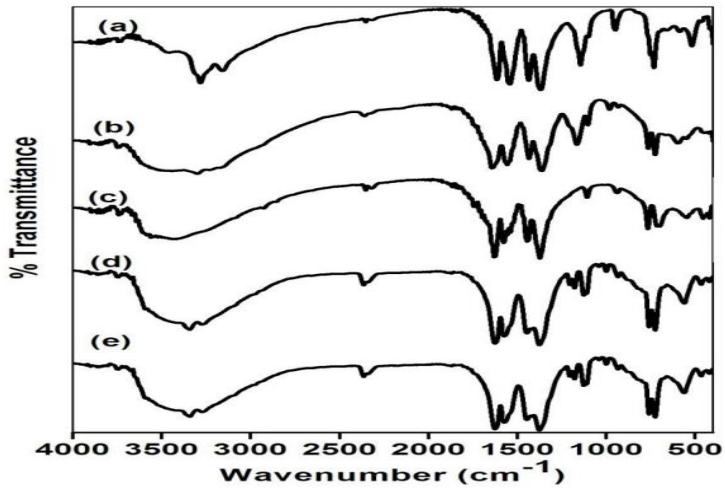

Fig. 4. FTIR spectra of M(Htma)(N2H4)2, where M = (a) Co, (b) Ni, (c) Mn, (d) Cu and (e) Zn.

3.3 Raman spectra

The perceived Raman spectra of metal trimesates and trimesic acid are displayed in Fig. 5. The emblems employed for the different oscillatory patterns are as subsequent: ν represents elongation oscillations, β denotes within-plane flexing patterns, and γ signifies beyond-plane flexing patterns. The infrared and Raman spectroscopic information and their designations are provided in Table 3.
The Raman spectrum of trimesic acid displays the distinctive elongation oscillations of the carbonyl cluster: ν(C=O) at 1648 cm–1, out-of-plane oscillations of the carboxylic cluster: γ(OH)COOH at 955 cm–1, and an elongation oscillation of the hydroxyl cluster (OH)COOH at 3085 cm–1. The spectrums of metal complexes do not display these distinctive bands, which demonstrates that the carboxylate groups are engaged in the coordination with metal. Substitution of the acidic hydrogen with a metallic cation induces a modification in the bond potencies of carboxylate clusters and additionally brings about a depletion of intermolecular hydrogen bonding, resulting in noticeable alterations in the infrared and Raman spectra of the metallic trimesates in comparison to those of trimesic acid.

For example, the bands caused by carboxylic group oscillations vanished in the complexes, while peaks originating from carboxylate anion oscillation are evident. In trimesic acid, the spectrum that arises from out-of-plane flexing modes of the ring double bond and a carboxylic group, γ(C=C)—c=c—, is observed at approximately 998 cm–1. This group is relocated towards elevated wavenumbers (approximately 1000 cm–1) in the spectra of compounds, indicating an increased electronic charge density surrounding the dual linkage (—C=C—) in trimesates compared to trimesic acid.
The bands perceived in the areas of ~1425 cm–1 and ~1590 cm–1 are caused by the elongation oscillations of the fragrant circle. These groups emerged at approximately equivalent wavenumbers both in the spectrum of trimesic acid and in the compounds. This implies that the fragrant system has not been disturbed significantly upon coordination of trimesic acid with metals through carboxylate groups.

Table 3 Raman spectral data (cm–1)
Assignments of selected bands (cm–1) occurring in the IR and Raman spectra of trimesic acid and cobalt(II), nickel(II), manganese(II), copper(II) and zinc(II) trimesates.

Trimesic acid		Co(Htma)(N2H4)2		Ni(Htma)(N2H4)2		Mn(Htma)(N2H4)2		Cu(Htma)(N2H4)2		Zn(Htma)(N2H4)2		Assignment
IR	Raman	IR	Raman	IR	Raman	IR	Raman	IR	Raman	IR	Raman	
3085vw	3077 w	-	-	-	-	-	-	-	-	-	-	(OH)COOH
1712 s	1648 s	-	-	-	-	-	-	-	-	-	-	(C=O)
-	-	1612 s	1596 m	1640 s	1609 m	1614 s	1631 s	1626 s	1605 m	1616 vs	1580 m	- as(COO)
1607 m	-	1523 vs	1545 m	1554 s	1554 m	1583 vs	-	1577 s	1545 w	1577 vs	-	(CC)ar
1455 s	1424 m	1435 vs	1420 s	1436 s	1449 s	1445 vs	1457 vs	1437 vs	1432 m	1442 s	1457 s	(CC)ar
-	-	1371 vs	1392 m	1363 vs	1365 m	1372 s	1363 w	1372 vs	1363 vw	1367 vs	1364 m	- s(COO)
1112 s	-	1151 m 1113 vw	1101 vw	1165 vs 1101 m	1061 m	1106 s	1155 vw	1181 vw	1097 s	1176 vw 1108 s	1171 vw	ß(CH)
955 vw	-	-	-	-	-	-	-	-	-	-	-	γ(OH)COOH
-	1000 vs	-	1001 vs	-	1002 vs	-	1002 vs	1007 m	998 vs	1002 w	1002 vs	γ(CH)-C=C-

Note: vs – very strong, s – strong, m – medium, w – weak, vw – very weak.

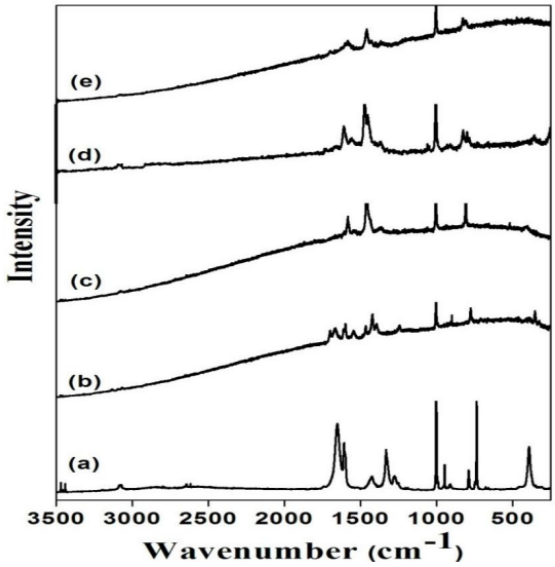

Fig. 5. Raman spectra of trimesic acid (a) and trimesates complexes of cobalt (b), nickel (c), manganese (d) and zinc (e).

3.4 EPR spectra

EPR spectra of solid samples of the compounds under investigation were recorded at ambient temperature. The specimens demonstrate EPR signals characteristic of the solitary entity with vertical symmetry. Illustrative EPR spectra of cobalt(II), copper(II), nickel(II), and manganese(II) compounds (solid specimen) at room temperature are depicted in Figure 3.6. The g∥ and g⊥ values were obtained from the EPR spectra of complexes using 2,2-diphenyl-1-picrylhydrazyl (DPPH) free radical as 'g' indicator and the acquired g values are showcased in Table 4. The EPR spectra exhibit lack of hyperfine splitting, which could be attributed to the circumstance that the paramagnetic centre is not diluted. For the copper compound, the detected g∥ magnitude (2.261) is greater than the g⊥ magnitude (1.834) indicating that the solitary electron is concentrated in the dx2−y2 orbital of the metal ions. It is in harmony with the reality that, for d9 system in deformed octahedral structure the solitary electron resides in the dx2−y2 orbital providing 2B1g as the fundamental state with g parallel > g perpendicular.

In accordance with Kivelson and Neiman,[21] the g value of < 2.3 suggests covalent quality of the metal–ligand bond and >2.3 signify ionic quality. Utilising these criteria to the 'g' values perceived for the complexes (Table 4), a covalent nature for the metal–ligand connection in the complexes under examination has been foreseen which is in accordance with the electronic spectral findings. According to Hathaway and Billing,[22] if the minimum g > 2.04 (either g∥ or g⊥) and G (defined as G = (g∥ – 2)/(g⊥ – 2)) is lower than 4, (i.e., g > 2.04 and G < 4) there is a noteworthy interchange interaction in the solid complexes; if the minimum g < 2.03, the metal ion may be in compressed tetragonal-octahedral stereochemistry. The patterns g⊥< ge (2.0023) < g∥ and the g⊥< 2.03 (g⊥ is minimum g in these compounds) observed for Co(II), Ni(II) and Cu(II) compounds imply that there is no interchange interaction in the solid compounds and these compounds have axially compressed octahedral structure.[22,23]

Table 4 EPR spectral data of the prepared complexes

Complex	g∥	g⊥	giso
Co(Htma)(N2H4)2	2.217	1.842	1.967
Ni(Htma)(N2H4)2	2.279	1.894	2.02
Mn(Htma)(N2H4)2	–	–	1.987
Cu(Htma)(N2H4)2	2.261	1.834	2.02

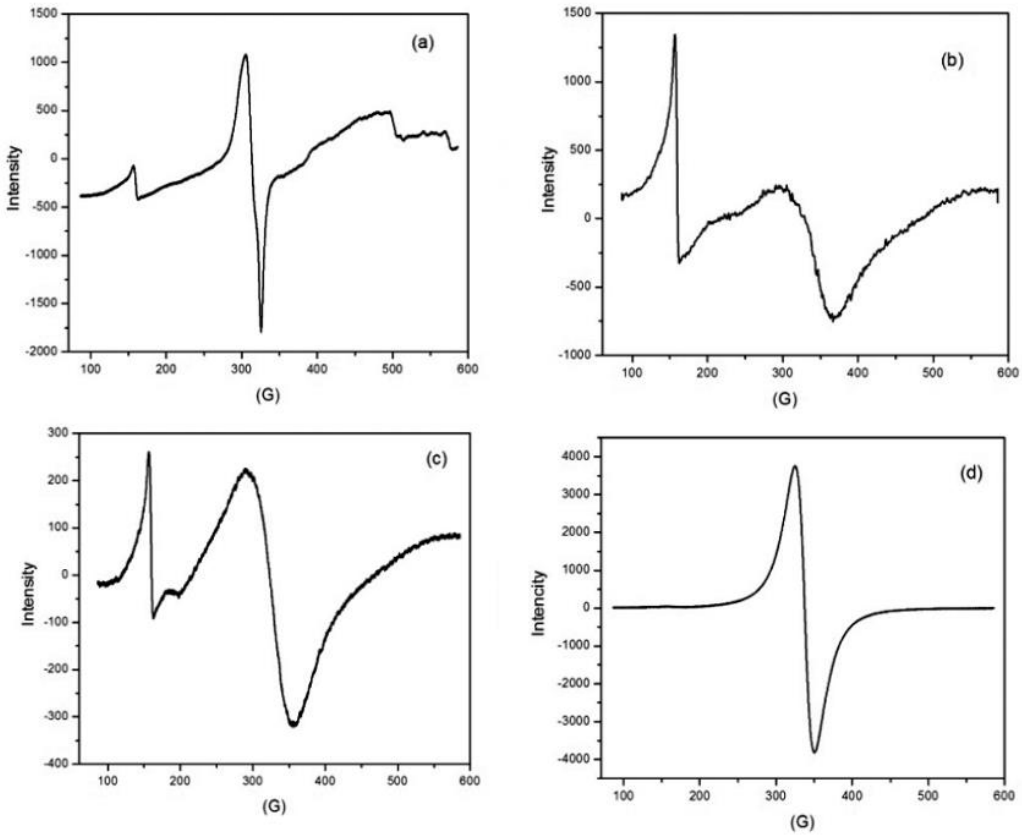

Fig. 6. EPR spectra of (a) Cu(II), (b) Co(II), (c) Ni(II) and (d) Mn(II) Complexes at RT.

3.5 Thermal decomposition studies

The concurrent TG–DTA diagrams of cobalt, copper, manganese, nickel and zinc compounds are displayed in Fig. 7 and the calorimetric data are provided in Table 5. By fitting the observed mass losses in TG with potential decomposition products, the compositions of the intermediates and the ultimate products were obtained [24-34]. The TG tracings of all the formulated compounds, M(Htma)(N2H4)2 where M = Cobalt, Nickel, Manganese, Copper and Zinc, exhibit three-stage degradation in accordance with DTA revealing either heat-absorbing or heat-releasing changes. In the preliminary phase, the compounds of Manganese, Nickel, and Zinc disintegrate exothermically at 85–290 °C with a weight reduction corresponding to two particles of hydrazine to yield the corresponding metal hydrogen trimesate as an intervening substance. However, the intricate combination of Cobalt and Copper disintegrate in an energetically demanding manner to shed a single hydrazine molecule during the initial phase, resulting in the formation of metal hydrazine hydrogen trimesate as an intervening substance. In the subsequent phase, the middle disintegrate (310–420 °C) to shed the organic components and produce the corresponding metal carbonates as the subsequent middle stage. In the ultimate phase, the metal carbonate intermediate additionally breaks down to generate corresponding metal oxide as the ultimate outcome.

Table 5 Thermal data

Complexes	DTA Temp./ °C	Thermogravimetry (TG)		Decomposition products
		Temp. range/°C	Mass loss/% Found(Calculated)	
Co(Htma)(N2H4)2	168(+)	73-236	8.3(9.6)	Co(Htma).N2H4
	331(+)	236-511	55.2(54.3)	CoCO3
	541(+)	511-857	15.7(13.2)	CoO
Cu(Htma)(N2H4)2	124(+)	66-165	10.4(9.5)	Cu(Htma)(N2H4)
	237(+)	165-282	8.2(9.5)	Cu(Htma)

	354(-)	282-538	53.8(54.2)	CuO
Mn(Htma)(N2H4)2	168(+) 560(+) 947(-)	44-313 313-656 656-979	20.1(19.5) 44.5(45.2) 13.1(13.4)	Mn(Htma) MnCO3 MnO
Ni(Htma)(N2H4)2	177(+) 297(+) 608(+)	82-269 269-539 539-931	18.8(19.3) 45.1(44.7) 14.5(13.2)	Ni(Htma) NiCO3 NiO
Zn(Htma)(N2H4)2	150(+) 415(-) 685(+)	51-287 287-631 631-970	18.1(18.9) 42.5(43.8) 13.8(14.2)	Zn(Htma) ZnCO3 ZnO

Note: (+) Endo thermic decomposition (-) Exo thermic decomposition

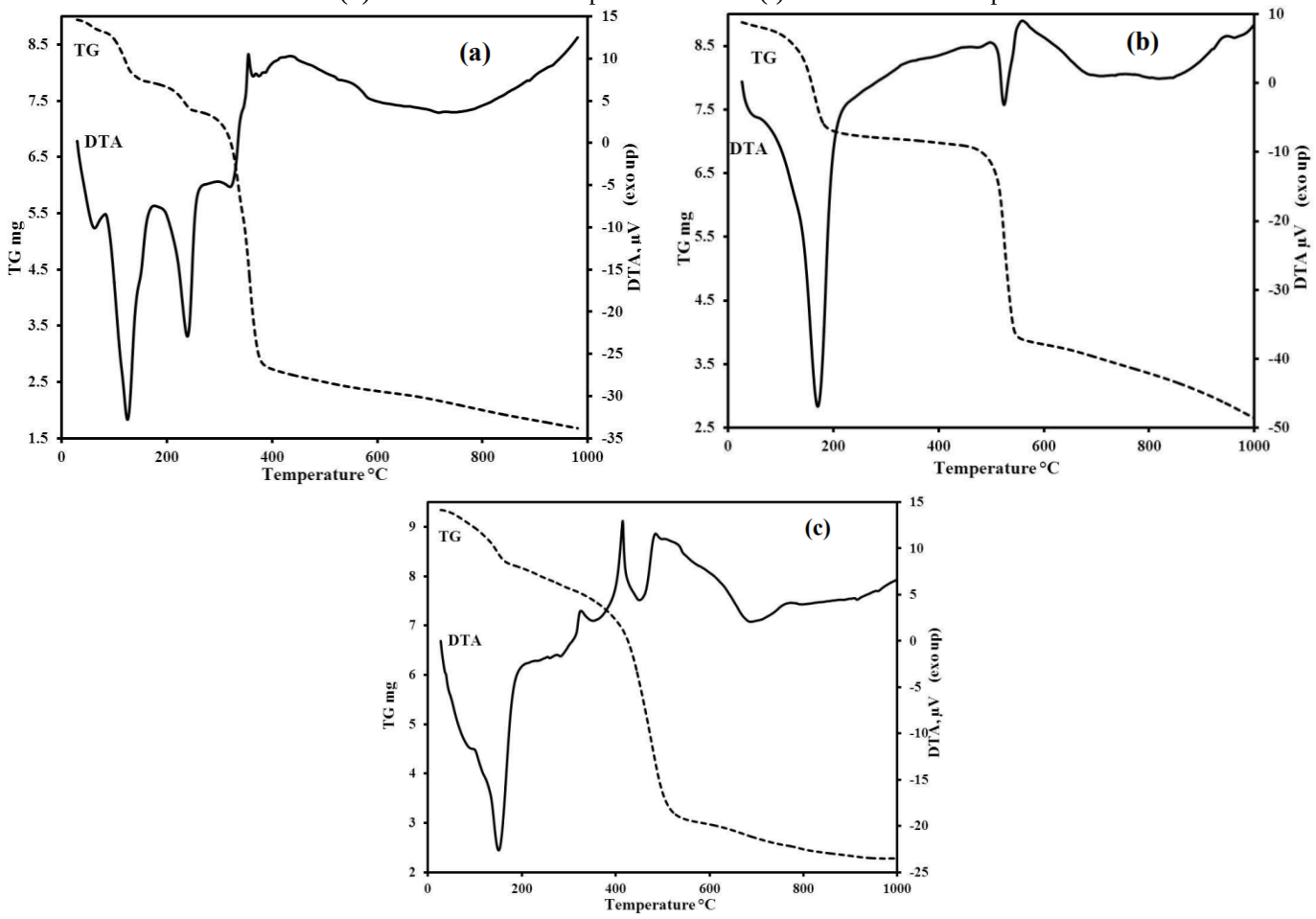

Fig. 7. Simultaneous TG–DTA curves of (a) Cu(Htma)(N2H4)2, (b) Mn(Htma)(N2H4)2 and (c) Zn(Htma)(N2H4)2.

3.6 Powder X-ray diffraction

The documented powder X-ray diffraction patterns of the compounds are displayed in Fig. 8. A juxtaposition of the XRD data of distinct complexes discloses that all the complexes display analogous XRD patterns, suggesting that the crystal structures of these complexes are congruous with one another. The summits detected at 2θ angles of 10.37°, 20.86°, 38.1°, and 42.39° for the Mn compound can be identified, correspondingly, to the (1 0 0), (2 0 0), (3 2 0), and (4 0 0) planes of the uncomplicated cubic crystal configuration.

X-ray diffraction (XRD) patterns of Co(II), Ni(II), Cu(II), and Zn(II) compounds are quite comparable, and all these compounds display peaks at 2θ angles of approximately 11.4°, 18.1°, and 26.0°, corresponding, respectively, to the (1 1 0), (2 1 0), and (3 1 0)

planes of a tetragonal crystal lattice. The magnitude of all the peaks is quite low, and less distinct patterns are observed in the 2θ range of 45–70°, indicating that the complexes might possess a polymeric arrangement or primarily amorphous character. Efforts to ready solitary crystals were not fruitful.

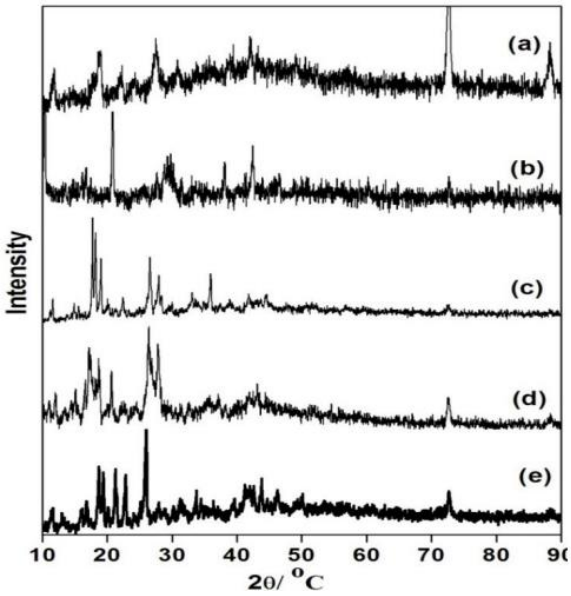

Fig. 8. Powder XRD patterns of the complexes M(Htma)(N2H4)2, where M = (a) Co, (b) Mn, (c) Ni, (d) Zn and (e) Cu.

3.7 SEM and EDAX studies

The compounds were incinerated in a kiln at their decomposition temperature and heated at 800 °C for 1 h to obtain the oxides of the elements, and subsequently, the structure and particle size of the oxides produced were examined. The SEM pictures of remnants acquired from Cu(Htma)(N2H4)2 and Mn(Htma)(N2H4)2 are displayed in Fig. 9 and the EDX diagrams obtained for these remnants (oxides) are provided in Fig. 10.

Based on the visuals, it is inferred that the remnants consist of approximately 500 nm sized metal oxide particles with consistent forms and the compounds could potentially serve as a precursor for nanometal oxides synthesis.[37] The EDX spectra provide the qualitative as well as quantitative analytical data regarding the samples. The EDX qualitative examination suggests the existence of corresponding metal oxides in the remnants of the compounds. The EDX spectral quantitative assessment suggests a metal: oxygen (M:O) stoichiometry of 1:1 in these remnants affirming the creation of NiO, CuO, MnO, and ZnO during the thermal degradation of these compounds. Based on the analytical and spectral findings, a six coordination octahedral structure has been tentatively suggested for the compounds (Fig. 11).

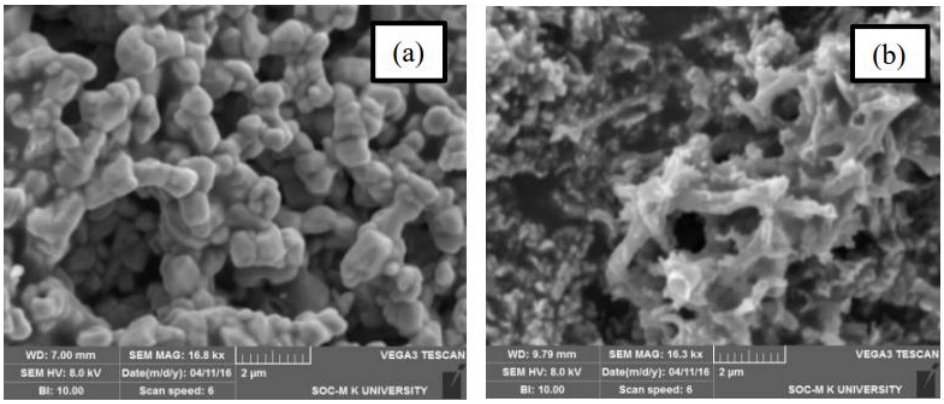

Fig. 9. SEM images of (a) CuO and (b) MnO obtained using Cu(Htma)(N2H4)2 and Mn(Htma)(N2H4)2 complexes.

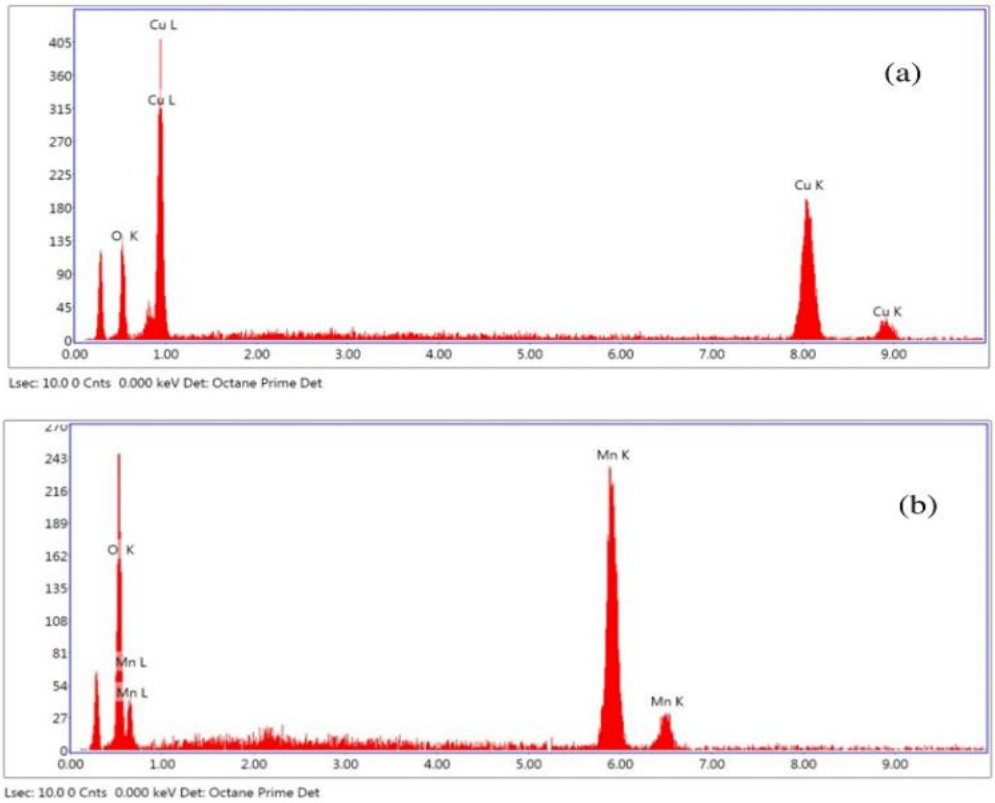

Fig. 10. EDX spectra of (a) CuO and (b) MnO obtained using Cu(Htma)(N2H4)2 and Mn(Htma)(N2H4)2 complexes.

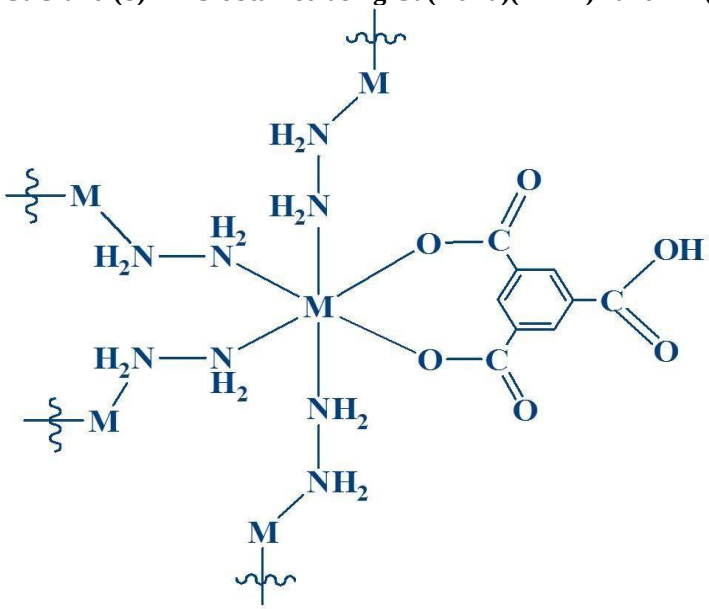

Fig. 11. Proposed structure of M(Htma)(N2H4)2 where M = Co, Ni, Cu, Mn and Zn.

3.8 Antimicrobial Activities

3.8.1 Antibacterial activity studies

The antibacterial actions of the ligand and the complexes of Mn(II), Co(II), Ni(II), Cu(II) and Zn(II) were checked on three Gram-negative bacteria viz., *Pseudomonas aeruginosa*, *Proteus mirabilis* and *Vibrio harveyi* and a Gram-positive bacterium *Staphylococcus aureus* by the disc diffusion technique. The zone of inhibition around each disk, after incubation, was measured in millimeter and presented in Fig. 12 and Table 6. It is clear from Fig. 12 that the growth inhibitions are much larger by metal complexes than by the bare ligand. The enhanced activity of the metal complexes can be explained on the basis of chelation theory.[38] The chelation tends to make the ligands act as more powerful and potent bactericidal agents, thus inhibits bacteria growth more than the bare ligand. The

Zn(II) complex showed remarkable activity against P. mirabilis, S. aureus and P. aeruginosa than other complexes. The Co(II) complex is highly active against P. aeruginosa microorganism. The Mn(II) complex has very low activity against all the four microorganisms.

Table 6 Antibacterial activity results of ligand and its metal complexes

Compound (1 mg/mL)	Growth Inhibition against Bacteria (diameter in mm)			
	P. aeruginosa	P. mirabilis	V. harveyi	S. aureus
H3tma	3	5	4	3
Co(Htma)(N2H4)2	26	10	9	10
Ni(Htma)(N2H4)2	10	-	10	10
Cu(Htma)(N2H4)2	12	10	12	12
Mn(Htma)(N2H4)2	-	-	-	-
Zn(Htma)(N2H4)2	20	16	14	32
Streptomycin (Std)	38	34	36	34

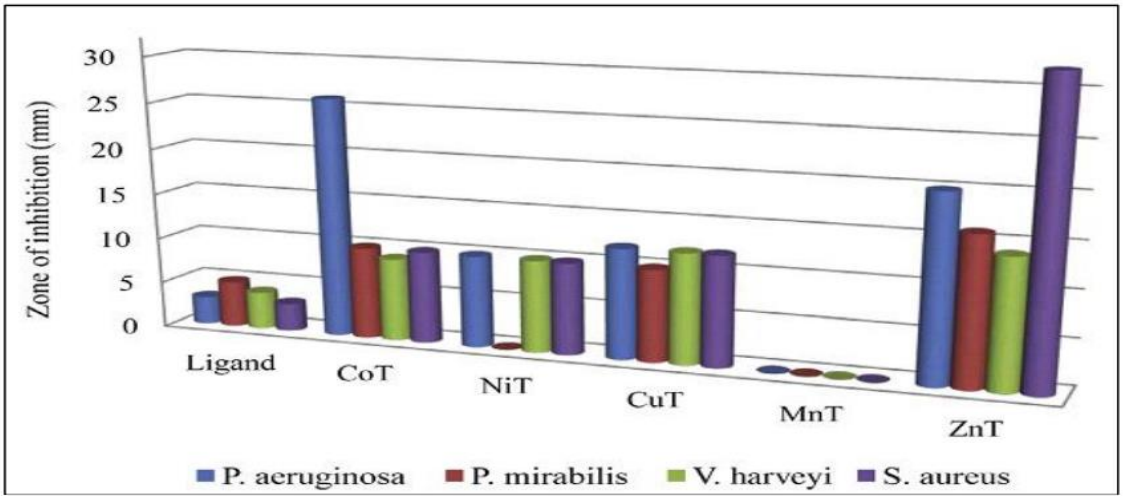

Fig. 12. Antibacterial activity of the ligand and complexes.

3.8.2 In vitro antifungal activity

In vitro antifungal activities of trimesic acid (H3tma) and its metal complexes were carried out against four fungi *Candida albicans*, *Aspergillus niger*, *Aspergillus fumigatus* and Penicilium variance and compared with standard antifungal drug Ketoconazole at the same concentration. Antifungal activity data are given in Table 7 and the mycelial growth of inhibition are presented in Fig. 13 and Fig. 14. The antifungal activity data showed hydrazine with transition metal complexes are more active compared than the free ligand. All the metal hydrazine complexes showed highly remarkable antifungal activity against the entire microorganism as compared to the activity of the reference drug Ketoconazole. Among all the prepared complexes, the complexes of Cu(Htma)(N2H4)2 and Zn(Htma)(N2H4)2 were the maximum active against all the tested fungi and exhibited the Zn(II) complex a greater activity (22mm) against P. variance. The effective antifungal activity of synthesized complexes compared to the corresponding ligand can be explained on the basis of chelation theory. The polarity of the metal ion will be reduced to a greater extent upon chelation due to the overlap of the ligand orbital and partial sharing of the charge of the metal ion with donor groups. It increases the delocalization of π-electrons over the whole chelating ring and enhances the penetration of the complexes into lipid membranes and block the metal binding sites in the enzymes of microorganisms. Thus, these complexes disturb the respiration process of the cell and block the synthesis of proteins, which restricts further growth of microorganism [39].

Table 7 In vitro antifungal screening data of the ligand, its metal complexes and the standard drug

Compounds (1 mg/mL)	Mycelial growth inhibition in mm			
	A. fumigatus	A. niger	P. variance	C. albicans
H3tma	12	8	11	10
Co(Htma)(N2H4)2	17	13	17	18
Ni(Htma)(N2H4)2	20	13	21	16
Cu(Htma)(N2H4)2	20	15	20	20
Mn(Htma)(N2H4)2	19	12	17	19
Zn(Htma)(N2H4)2	19	15	22	18
Ketoconazole (Std)	23	16	24	21

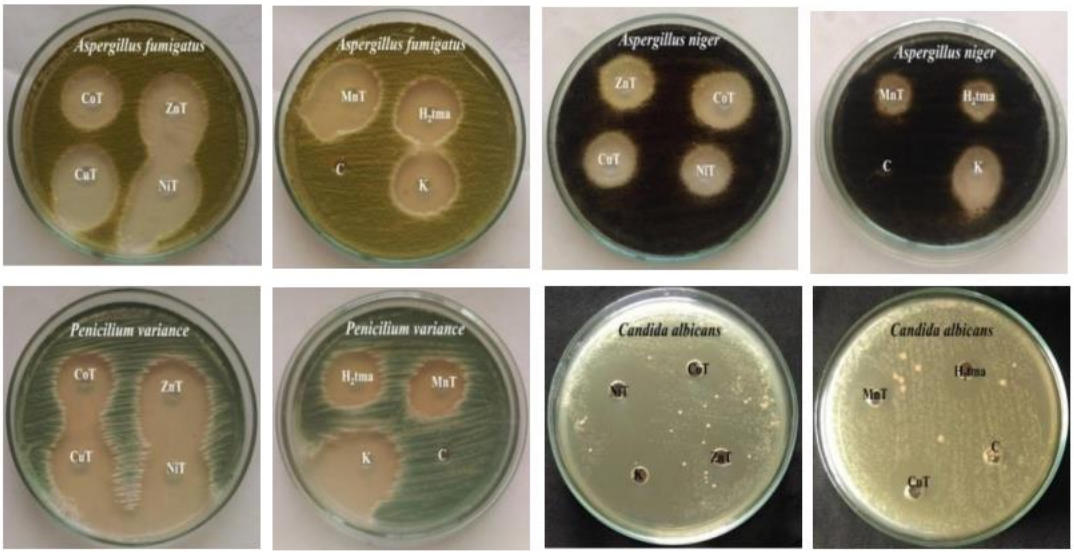

Fig. 13. Antifungal action of ligand and metal complexes (well diffusion method).

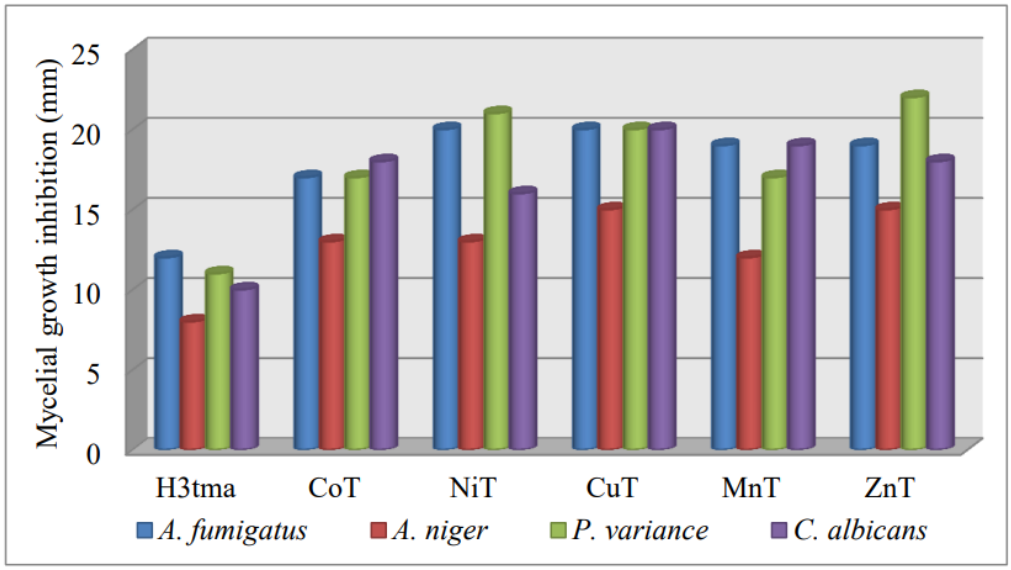

Fig. 14. Antifungal activity of the ligand and complexes.

Conclusions

This study presents the successful synthesis and characterization of novel trimesic acid and hydrazine mixed-ligand complexes with Mn(II), Co(II), Ni(II), Cu(II), and Zn(II). Spectroscopic studies, including FTIR, Raman, and EPR, confirmed the octahedral geometry and coordination patterns. Thermal decomposition studies identified these complexes as precursors for nano-metal oxides, with significant implications for nanomaterial synthesis. The complexes displayed enhanced antibacterial and antifungal activities, attributed to increased bioavailability from chelation, as explained by chelation theory. Notably, Zn(II) and Cu(II) complexes demonstrated exceptional antimicrobial efficacy, surpassing the free ligand and comparable to standard drugs. These findings suggest the potential utility of these complexes in biomedical applications and advanced material synthesis. Future research could explore their catalytic properties and detailed mechanisms of biological activity.

References

1. J.W. Steed, J.L. Atwood, Supramolecular Chemistry, second ed., Wiley, New York, 2000.
2. J.P. Sauvage, Transition Metals in Supramolecular Chemistry, 5, Wiley, New York, 1999.
3. A.R. Millward, O.M. Yaghi, J. Am. Chem. Soc. 127 (2005) 17998–17999.
4. A.Muller, Y. Zhou, H. Bogge, M. Schmidtmann, T. Mitra, E.T.K. Haup, A. Berkle, Angew. Chem. Int. Ed. 45 (2006) 460–465.
5. B.N. Sivasankar, S. Govindarajan, Synth. React. Inorg. Met.-Org. Chem. 24 (1994) 1573–1582.
6. B.N. Sivasankar, S. Govindrajan, Synth. React. Inorg. Met.-Org. Chem. 24 (1994) 1583–1597.
7. T. Premkumar, S. Govindarajan, J. Therm. Anal. Calorim. 100 (2010) 725– 732.
8. L. Vikram, B.N. Sivasankar, J. Therm. Anal. Calorim. 91 (2008) 963–970.
9. L.R. Gonsalves, V.M.S. Verenkar, S.C. Mojumdar, J. Therm. Anal. Calorim. 96 (2009) 53–57.
10. Z. Rzqczynska, A. Ostasz, S. Pikus, J. Therm. Anal. Calorim. 82 (2005) 347– 351.
11. F. Ying, L. Guobao, L. Fuhui, X. Ming, L. Jianhua, J. Mol. Struct. 1004 (2011) 252–256.
12. C. Zhenfeng, R. Huijuan, L. Guixia, H. Guangyan, J. Rare Earths 24 (2006) 724–727.
13. J.X. Chen, S.X. Liu, E.Q. Gao, Polyhedron 23 (2004) 1877–1888.
14. A.B.P. Lever, Inorganic Electronic Spectroscopy, 2nd ed., Elsevier, Amsterdam, 1894.
15. A.B.P. Lever, J. Chem. Educ. 45 (11) (1968) 711.
16. K. Nakamoto, Infrared and Raman Spectra of Inorganic and Coordination Compounds, Wiley, New York, 1978.
17. A.Braibanti, F. Dallavalle, M.A. Pellingheli, E. Laporati, Inorg. Chem. 7 (1968) 1430–1433.
18. G. Varsanyi, M.A. Kovner, L. Lang, Assignments for Vibrational Spectra of 700 Benzene Derivatives, Akademia Kiado, Budapest, 1973.
19. M. Kalinowska, J. Piekut, A. Bruss, C. Follet, J.S. Gromiuk, R. Swislocka, Z. Rzaczynska, W. Lewandowski, Spectrochim. Acta A 122 (2014) 631–638.
20. S.X. Min, W.H. Yan, L.Y. Bing, Y.J. Xiu, C. Lei, H. Ge, X.W. Qing, Z. Bing,
21. Chem. Res. Chin. Univ. 26 (2010) 1011–1015.
22. D. Kivelson, R. Neiman, J. Chem. Phys. 35 (1961) 149.
23. B.J. Hathaway, D.E. Billing, Coord. Chem. Rev. 5 (1970) 143–207.
24. B.J. Trzebiatowska, J. Lisowski, A. Vogt, P. Chemielewski, Polyhedron 7 (1988) 337–343.
25. V. Jordanovska, R. Trojko, Thermochim. Acta 258 (1995) 205–217.
26. H. Icbudak, T.K. Yazicilar, V.T. Yilmaz, Thermochim. Acta 335 (1999) 93– 98.
27. U.B. Gawas, V.M.S. Verenkar, Thermochim. Acta 556 (2013) 41–46.
28. K. Saravanan, S. Govindarajan, D. Chellappa, Synth. React. Inorg. Met.-Org. Chem. 34 (2004) 353–369.
29. S. Yasodhai, S. Govindarajan, Synth. React. Inorg. Met.-Org. Chem. 29 (1999) 919–934.
30. B.N. Sivasankar, S. Govindarajan, Mater. Res. Bull. 31 (1996) 47–54.
31. K. Saravanan, S. Govindarajan, J. Chem. Sci. 114 (2002) 25–36.
32. T. Premkumar, S. Govindarajan, Thermochim. Acta 386 (2002) 35–42.
33. S. Vairam, T. Premkumar, S. Govindarajan, J. Therm. Anal. Calorim. 100 (2010) 955–960.
34. K. Kuppusamy, S. Govindarajan, Thermochim. Acta 274 (1996) 125–138.
35. S. Vairam, T. Premkumar, S. Govindarajan, J. Therm. Anal. Calorim. 101
36. (2010) 979–985.
37. L. Vikram, B.N. Sivasankar, Thermochim. Acta 452 (2007) 20–27.
38. S. Yasodhai, S. Govindarajan, J. Therm. Anal. Calorim. 62 (2000) 737–745. 37.
39. K.C. Patil, J. Chem. Sci. 96 (1986) 459–464.